Pathway Studies in Si(2p) Inner-Shell Processes of $H_2Si(CH_3)_2$ by Mass Spectrometry and the Photoion−Photoion Coincidence Method in the Range 24−133 eV

Bong Hyun Boo,*,† Zhaoyang Liu,† and Inosuke Koyano‡

Department of Chemistry, Chungnam National University, Taejon 305-764, Korea, and Center for Molecular Science, 373-1 Kusung-dong, Yusung-gu, Taejon 305-701, Korea, and Department of Material Science, Himeji Institute of Technology, 1479-1 Kanaji, Kamigohri, Hyogo 678-12, Japan

Received: April 29, 1999

Dissociative multiple photoionization processes of dimethylsilane ($H_2Si(CH_3)_2$) have been investigated in the valence and Si(2p) core level photoexcitation/photoionization regions by time-of-flight (TOF) mass spectrometry coupled to synchrotron radiation, operated in both the photoelectron−photoion coincidence (PEPICO) and photoion−photoion coincidence (PIPICO) modes. Two group absorption bands below and above the $Si(2p_{3/2})$ threshold 106.51 eV are observed in both total photoion and PIPICO yield curves. Various monocations of $H_n^+(n = 1-3)$, $CH_n^+(n = 0-4)$, $C_2H_n^+(n = 1-3)$, $SiH_n^+(n = 0-3)$, $SiCH_n^+(n = 0-5)$, $SiC_2H_n^+(n = 0-7)$ are observed, the yields depending on the excitation energy. In the valence ionization region, especially $E <$ 30 eV, extrusions of H, H_2, CH_3, and of CH_4 (or H + CH_3) and CH_3 + H_2 (or H + CH_4), are predominantly observed leading to the formation of $SiC_2H_n^+$ ($n = 6, 7$) and $SiCH_n^+$ ($n = 3-5$), respectively, whereas in the Si(2p) excitation and ionization regions, ionic fragments of smaller masses such as H^+, CH_3^+, Si^+, and $SiCH_3^+$ are relatively abundant in the PEPICO spectra. Bond-selective fragmentation processes occur in the two absorption regions. An ab initio calculation was also carried out to predict discrete excitation energies and their modes corresponding to the transitions from the core to valence and Rydberg orbitals.

Introduction

In recent years, extensive studies have been made of the energetics, spectroscopy, and dynamics of the core-hole excited states involving Si(1s),[1−3] Si(2s),[3] and Si(2p)[3−32] cores by various methods such as X-ray photoabsorption spectroscopy,[1−3] discrete variational (DV)$X\alpha$ method,[22] multiple-scattering (MS) $X\alpha$ method,[23] and electron energy loss spectroscopy.[24] The interpretation of the photoionization mass spectra of molecules is of much importance to infer the electronic and charge states of the parent ions. Also, the coincident detection of ion pairs formed via the absorption of the single VUV photon leads to insight into the dissociation pathways and repulsive states as well as the identification of the charge states of the precursor ions. The photoion−photoion coincidence (PIPICO) technique has been frequently employed to probe two ionic fragments formed via dissociative ionization of gas molecules, and sometimes to measure kinetic energy release in the fragmentation.

In our previous study, we reported dissociation patterns of multiply charged trimethylsilane (TMS, $HSi(CH_3)_3$), both in the valence and Si(2p) core level excitation/ionization regions, in the photon energy range 38−133 eV.[5] In that report, we could not clarify fragmentation pattern details because we could not resolve some individual ions owing to the overlap between the adjacent masses, the *m*/*z* ratio differences of which are one or two. The mass overlap occurs greatly in the mass spectral region of $SiC_nH_p^+$ ($n \geq 1$) ions at high excitation energy, because TMS includes three carbon atoms, and thus there could exist a variety of dissociation patterns. At high energy involving excitation of the Si(2p) shielding electron, the time-of-flight (TOF) signals are broad owing to the kinetic energy release via Coulomb explosion decomposition. However, by employing a relatively more simple molecule such as dimethylsilane (DMS, $H_2Si(CH_3)_2$), in which fewer carbon atoms are bonded to silicon, we could better resolve each mass and thus elucidate the energy variation of dissociation behaviors in more detail. Furthermore, we could directly compare reactivities such as the H and CH_3 eliminations, because an equal number of H atoms and methyl groups are involved in the molecule.

In an attempt to clarify the dissociation mechanism, we have also checked the pressure effect on various ion yields, because this kind of experiment could verify that the individual product ions are formed via a single collision between a photon and a molecule. An ab initio calculation was also performed to predict the energies and symmetries of the excited states arising from the core excitation. Bond-selective fragmentation patterns are discussed in conjunction with the relevant electronic states.

Experimental and Theoretical Section

The present experiments were carried out using a TOF mass spectrometer, coupled to a constant-deviation grazing incidence monochromator installed at the BL3A2 beam line of the Ultraviolet Synchrotron Orbital Radiation (UVSOR) facility in Okazaki. The design and construction of the apparatus have been described in detail elsewhere,[33,34] and thus are only briefly described here. The dispersed photon beam enters the ionization region through a hole (3 mm ø). A relatively high electric field

* To whom correspondence should be addressed. E-mail: BHBoo@hanbat.chungnam.ac.kr.
† Chungnam National University and Center for Molecular Science.
‡ Himeji Institute of Technology.

10.1021/jp991413t CCC: $19.00
Published on Web 02/02/2000

(725 V/cm) was applied to the ionization chamber having a 6-mm-diameter hole for ion extraction. The entrance aperture of the drift tube was 8 mm in diameter. The TOF mass spectrometer employs a drift tube of adjustable length for a facile detection of metastable ions or to obtain better resolved mass spectra. Flight-path lengths of 20 and 50 cm were used in the present study. The mass detection angle can be varied by rotating the mass spectrometer in the plane perpendicular to the incident photon beam direction. In this study, a quasi-magic angle of 55°[35,36] between the ion flight path axis and the polarization direction of the synchrotron beam is used for suppression of anisotropic effect in the collection of fragment ions.

The TOF mass spectrometer is operated by the time-correlated ion-counting technique in two different modes: a PEPICO mode and a PIPICO mode. To operate the PEPICO mode, the start pulses for a time-to-amplitude converter (TAC) are provided by the photoelectron signals at a channel electron multiplier, sampled from the collision chamber in the opposite direction of the ion flight direction, and the stop pulses are generated by the photoion signals at microchannel plates located at the end of the TOF tube. To operate the PIPICO mode, however, the start pulses are provided by the lighter ions, and the stop pulses are generated by the heavier ions of counterparts.

Variation of the total PIPICO intensity with photon energy is obtained by recording PIPICO count rates and photon intensities while the photon wavelength is scanned. Normalized total PIPICO intensity is then obtained by dividing the recorded PIPICO count rates by the recorded photon intensities. When we measured the PIPICO count rates, the coincidence time range (gate width in TAC) was set to be 0−5 μs at the 20-cm flight path length (0−10 μs at the 50-cm flight path length), because the TOF differences between any pairs of ions formed from DMS fall into these time ranges.

A thin optical filter of aluminum was used in the energy range 38−68 eV for elimination of higher-order radiation. The slit width of the monochromator was 500 μm to give optical resolutions of 0.1 and 0.2 nm in the regions above and below 50 eV, respectively. The background pressure of the main chamber was $\approx 3 \times 10^{-9}$ Torr. When the DMS gas was introduced to the ionization chamber, the pressure of the main chamber was maintained at $\approx 6 \times 10^{-7}$ Torr. However, the sample gas pressure in the ionization region was not directly measured. The DMS gas was purchased from the Tori Chemical Research Institute Ltd. with a purity of 99.9999+ wt/wt % and was used without further purification. The TOF spectra confirmed its purity.

To assign all the resonance bands, ab initio molecular orbital calculations were carried out. To check the reliability of several ab initio calculations in predicting the structure and energies of DMS, the molecular geometry was optimized at the HF/6-31G*, MP2/6-31G*, and MP2/6-311G(2df,p) levels of theory, and then compared with the experimental geometry.[37] For the MP2 calculations, the core electrons are excluded for electron correlation calculation to reduce a computation time. The term values of the core-excited state, i.e., the energy difference between the core-excited state and the corresponding ionization limit, are estimated by the equivalent ionic core valence orbital model (EICVOM) calculation.[20,38] The HF/6-311++G(2df,p) orbital energy calculations were performed on $H_2P(CH_3)_2^+$ at the experimental geometry of $H_2Si(CH_3)_2$,[37] and simply the negative values of the resulting unoccupied orbital energies were taken in this study as the term values of DMS. A Gaussian 94 program suite[39] installed at SERI of ETRI in Korea was used in these ab initio calculations. The various peaks in the total photoion and PIPICO yield curves are compared with theoretical evaluation by combining the computed term values, the experimental ionization limit for $Si(2p_{3/2})$, 106.51 eV,[19] and the energy difference between the binding energies of $Si(2p_{3/2})$ and $Si(2p_{1/2})$, 0.617 ± 0.005 eV.[19]

TABLE 1: Electronic Configuration of $H_2Si(CH_3)_2$ Determined by the HF/6-311++G(2df,p) Calculation

orbital involved	symmetry and numbers of electrons occupied
Si(1s)	$(1A_1)^2$
C(1s)	$(1B_2)^2$, $(2A_1)^2$
Si(2s)	$(3A_1)^2$
Si(2p)	$(1B_1)^2$, $(4A_1)^2$, $(2B_2)^2$
valence MO	$(5A_1)^2$, $(3B_2)^2$, $(6A_1)^2$, $(2B_1)^2$, $(7A_1)^2$, $(4B_2)^2$, $(1A_2)^2$, $(3B_1)^2$, $(8A_1)^2$, $(5B_2)^2$

TABLE 2: Geometrical Parameters of $H_2Si(CH_3)_2$ Optimized at the HF/6-31G*, MP2/6-31G*, and MP2/6-311G(2df,p) Levels

	calcd, Å			
parameters	HF/6-31G*	MP2/6-31G*	MP2/6-311G(2df,p)	exptl[a]
SiH	1.481	1.491	1.484	1.483
CSi	1.889	1.885	1.875	1.867
CH	1.087	1.094	1.092	1.095
HSiH	107.45	107.53	107.82	107.83
CSiC	111.41	111.09	110.89	110.98
CSiH	109.47	109.54	109.52	109.48
HCH	107.62	107.76	107.87	108.00

[a] Reference 34.

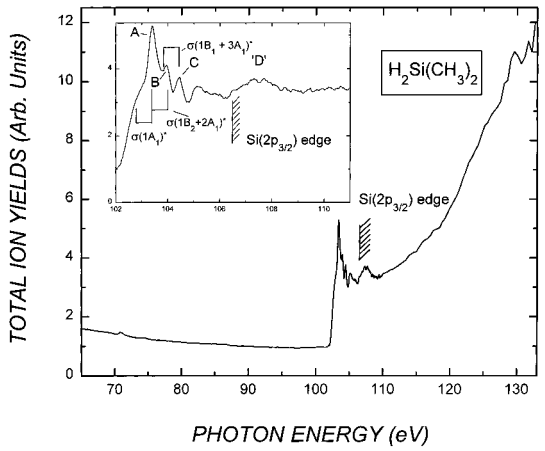

Figure 1. Total photoionization efficiency curve of $H_2Si(CH_3)_2$ recorded in the range of 65−133 eV. The inset shows the scale-expanded spectrum in the Si(2p) excitation region.

Results and Discussion

In the independent particle description, the ground-state electronic configuration of DMS can be written with the orbital ordering presented in Table 1, with the aid of the HF/6-311++G(2df,p) calculation. The geometrical parameters were optimized at the HF/6-31G*, MP2/6-31G*, and MP2/6-311G-(2df,p) levels. Table 2 lists the optimized geometrical parameters. Among the geometrical structure calculations, the MP2/6-311G(2df,p)-optimized geometry is found to be in better agreement with a microwave study[37] than other calculations.

In Figure 1 we present the total photoion yield as a function of energy in the range 65−133 eV. We present only the spectral region from 65 to 133 eV, because one of the three gratings covers only this energy range and it is adequate to show only a spectrum taken at the same conditions. In the total ion yield curve, we have observed a sharp rise from ≈ 102 eV. The binding energy of the $Si(2p_{3/2})$ electron has been reported as 106.51 eV, the value determined by high-resolution photoelec-

tron spectroscopy.[19] Hence, the transitions below 106.51 eV are attributed to the discrete excitation of the Si(2p) core electron to the unoccupied antibonding and Rydberg orbitals. Previous studies show that the excitation of Si(2p) core electron to the first antibonding orbital occurs when the incident photon energy reaches ≈ 103 eV, the energy being more or less shifted with different ligands.[3−28,30−32] Chemical shifts of photoelectron and Auger lines are linearly dependent on the average differences in Pauling's electronegativities to the nearest neighbors, $\Delta\bar{\chi}_P$.[40] Below the threshold, Morin et al. proposed that the double-resonant Auger process is more important than the direct double ionization below the Si(2p) edge.[12] This is discussed further below.

Above the threshold, we observe a small feature in the total ion yield curve which may correspond to a shape resonance near 107.6 eV (peak D), and also a slow rise above 109 eV, assigned to the delayed onset phenomena and/or to photoionization shake-off which never declines up to 133 eV, the maximum energy examined here. The post-threshold behavior of DMS is quite different from that of TMS, in which the total ion yield declines after 121.6 eV.[5]

The peak at ≈ 107.6 eV (peak D) may correspond to the shape resonance above the Si(2p) threshold coupled to the Rydberg orbitals and continuum. The resonance arises from the excitation of the Si(2p) to a quasi-bound potential well which is created by the backscattering of the excited electrons by ligands.

The slow rise may correspond to the delayed onset phenomena in the atomic photoabsorption and photoionization. This spectral behavior has also been observed in the photoionization of SiH_4.[30] The behavior is caused by centrifugal barrier effects which are increasingly important with the increasing angular momentum of the quantum number *l* involved.[41,42] However, one can speculate that the slow rise comes from dissociation following direct double photoionization, such as shake-off above the threshold, in which photoejection of an electron from the core gives rise to a sudden change in the central potential.[43,44] Mukoyama et al. reported the calculated atomic excitation probability for various shells as the result of a sudden Si(2p) vacancy production of the silicon atoms.[44] The electron excitation probability for 3s and 3p electron ejection accompanying a sudden Si(2p) ejection is estimated as 5.0 and 14.7%, respectively. For this molecule, double or multiple photoejection could occur with probabilities not less than those for the silicon atom as the result of the sudden vacancy of a Si(2p) shielding electron. This shake-off process can lead to the observation of many ionic fragments. In this region, the coincident ion pair formation of $H^+ - CH_n^+$ ($n = 0-3$) prevails, indicating that the possibility of triple ionization followed by molecular fragmentation is greatly enhanced.

A simple ab initio method is well-known to be able to estimate the orbital energies of core-hole excited molecules. By the EICVOM theory,[20,38] $H_2P(CH_3)_2^+$ corresponds to the equivalent ionic core of the core-excited state of DMS by assuming that the Si(2p) electrons effectively screen the nuclear charge, as in the case of the Si(1s) electrons. An ab initio calculation at the HF/6-311++G(2df,p) level has been performed on $H_2P(CH_3)_2^+$ to estimate the antibonding and Rydberg orbitals of the core-hole excited state of $H_2Si(CH_3)_2$. All the calculated results are listed in Table 3. However, the closely spaced intervals of term values hamper a straightforward assignment of the excitation energies. The excitation energy corresponding to $Si(2p_{1/2})$ -to-$\sigma(1A_1)$* can be estimated as 104.4 eV from the excitation energy calculated here, 103.83 eV (Table 3), and from the spin−orbit splitting, 0.617 ± 0.005 eV, determined in the spectra for SiX_4 (X = H, CH_3, F, Cl, etc.).[19] Peak A at 103.4 eV in Figure 1 may correspond to the $Si(2p_{1/2}) \rightarrow \sigma(1A_1)$* transition. The discrepancy between theory and experiment may reflect that the HF/6-311++G(2df,p) calculation may greatly underestimate the term values corresponding to the transition, although the Si(2p) electrons cannot efficiently screen the nuclear charge owing to the extensive d character. It is shown in previous literature that the term values determined by the configuration interaction calculation match better with experiment than do those determined by the HF calculation.[2,7] However, it should be pointed out that calculated term values suppose two separate calculations, one of the initial state and one of the final state, and therefore our simple calculation of virtual orbital energies by using the EICVOM theory could only help to assign the discrete excitation states.

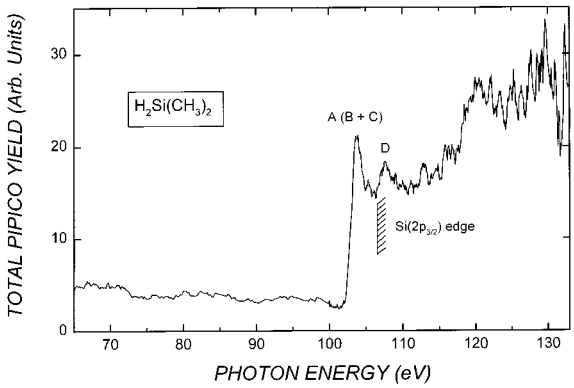

Figure 2. Total photoion−photoion yield curve of $H_2Si(CH_3)_2$ in the range of 65−133 eV.

TABLE 3: Excitation Energies (eV) for Various $Si(2p_{3/2})$ Core-Hole States of $H_2Si(CH_3)_2$ Determined by the HF/6-311++G(2df,p) Calculation

sym of orbital involved	Energy	sym of orbital involved	Energy
$1A_1$	103.83	$4A_1$	105.56
$1B_2$	104.31	$2B_2$	105.59
$2A_1$	104.47	$1A_2$	105.99
$1B_1$	104.70	$3B_2$	106.00
$3A_1$	105.02	$3B_1$	106.37
$2B_1$	105.33		

Peak B may arise from the $Si(2p_{1/2})$ -to-$\sigma(1B_2)$* and/or $Si(2p_{1/2})$ -to-$\sigma(2A_1)$* transitions. The excitation energy for these transitions is estimated as ≈ 105.0 eV, the value determined from the calculated excitation energy listed in Table 3 and the energy difference of the $Si(2p_{3/2})$ and $Si(2p_{1/2})$. The value is in fair agreement with the experimental value of 104.0 eV. Peak C may correspond to the transitions of $Si(2p_{1/2})$ -to-$\sigma(1B_1)$* and/or $Si(2p_{1/2})$ -to-$\sigma(3A_1)$*, the excitation energy of which is estimated as ≈ 105.5 eV, in fair agreement with an experimental value of 104.5 eV.

The total PIPICO efficiency curve is presented in Figure 2. The two features at ≈ 104 (Peaks A, B, and C) and ≈ 108 eV (Peak D) also appear, indicating that two kinds of resonances occur.

Figure 3 shows a typical PEPICO spectrum taken in the PEPICO mode, recorded at the 110-eV photon energy and the 50-cm flight path length. Unless otherwise noted, all the PEPICO and PIPICO spectra were taken at 20-cm flight path length. Various monocations, H_n^+ ($n = 1-3$), CH_n^+ ($n = 0-4$), $C_2H_n^+$ ($n = 1-3$), SiH_n^+ ($n = 0-3$), $SiCH_n^+$ ($n = 0-5$), and $SiC_2H_n^+$ ($n = 0-7$), are clearly observed.

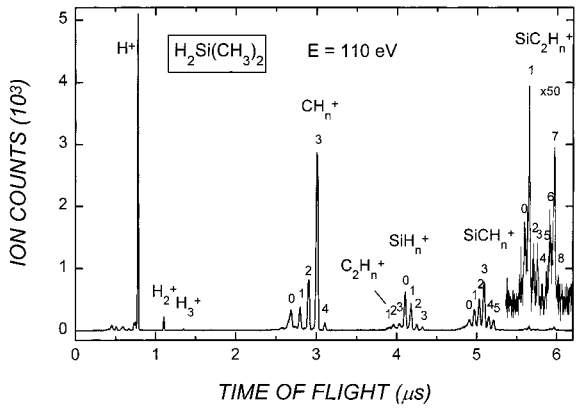

Figure 3. A typical PEPICO spectrum of $H_2Si(CH_3)_2$ measured at 110-eV photon energy and 50-cm TOF tube length. TOF axis is 55° with respect to the photon beam polarization.

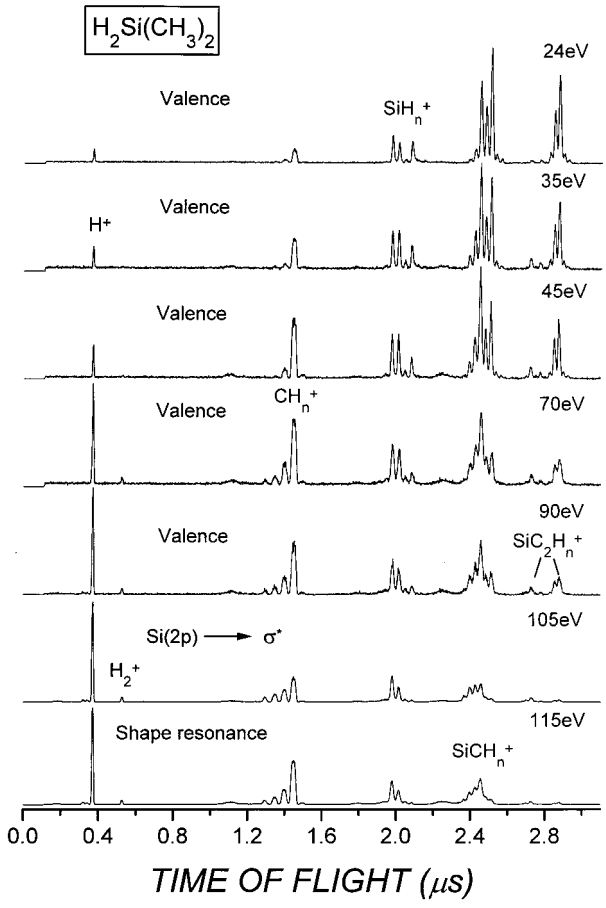

Figure 4. PEPICO spectra of $H_2Si(CH_3)_2$ taken by excitation at photon energies 24, 35, 45, 70, 90, 105, and 115 eV.

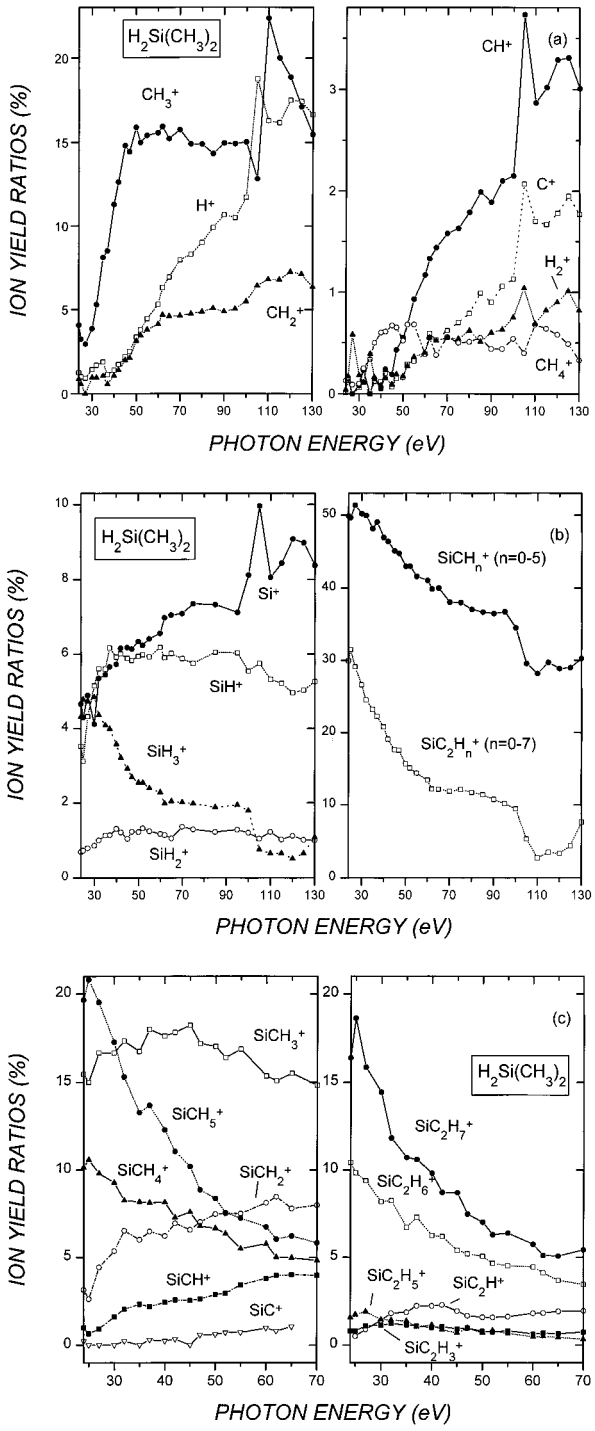

Figure 5. Ratios of integrated intensities of ion peaks in TOF mass spectrum of total photoion intensity ($I_{photoion}$:$I_{tot\ photoion}$) for $H_2Si(CH_3)_2$ as a function of photon energy.

In Figure 4, we present PEPICO spectra taken at 24, 35, 45, 70, 90, 105, and 115 eV. The variation of the ion yield ratio, $I_{photoion}$:$I_{tot\ photoion}$, with energy is shown in Figure 5a−c. It should be verified that the ions observed are formed from a single collision between a photon and a molecule. Therefore, we carried out several pressure-dependent experiments by varying the pressure of the sample. No appreciable variation of the individual ion yield ratios with pressure was observed. This indicates that each observed ion is formed from a single molecular process. The individual ion yield ratios in the four consecutive pressure-dependent experiments range as follows: H^+, 0.291 ± 0.011; H_2^+, 0.015 ± 0.001; H_3^+, 0.002 ± 0.001; CH_n^+, 0.430 ± 0.018; SiH_n^+, 0.101 ± 0.009; $SiCH_n^+$, 0.146 ± 0.010; $SiC_2H_n^+$, 0.016 ± 0.009. Here, the uncertainties of the ion yield ratios are 2σ (σ = standard deviation). In Figure 6a,b are presented the relative ion yields as a function of photon energy. It is also noticed that at a given energy, the relative yields are derived by multiplying the value for $I_{tot\ photoion}$:$I_{tot\ photon}$ (Figure 1) by the value for the corresponding ion yield ratio presented in Figure 5a−c. Therefore, the sum of intensities for all the ions indicated in Figure 6a,b equals the total photoion intensities displayed in Figure 1.

Figure 7 presents a well-resolved PIPICO spectrum taken at the 110-eV energy and the 50-cm flight path length. It should also be noted that the PIPICO spectrum was taken under the

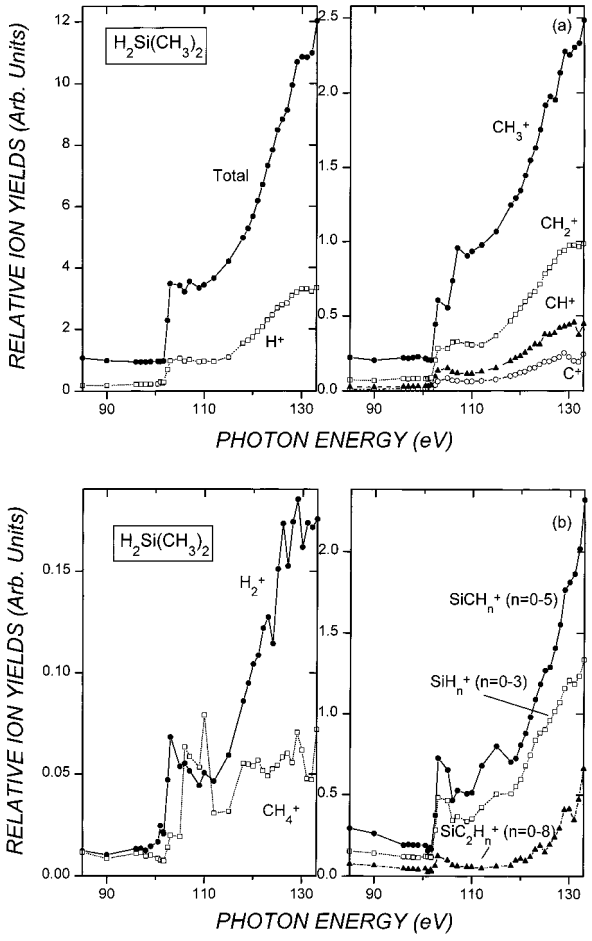

Figure 6. Partial ion yield spectra of $H_2Si(CH_3)_2$ in the range of 85−133 eV. The spectral intensities ($I_{photoion}$:$I_{tot\ photon}$) are presented on the same relative intensity scale.

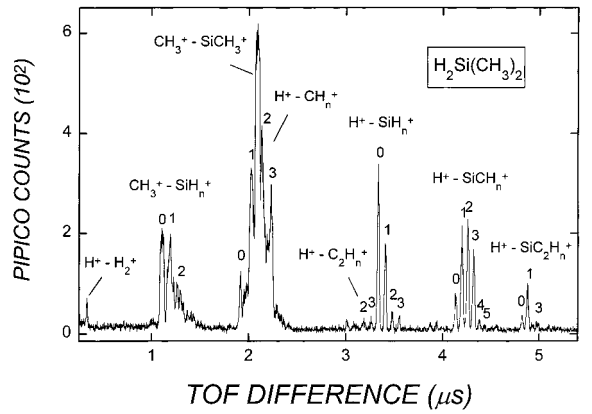

Figure 7. PIPICO spectra of $H_2Si(CH_3)_2$ measured at 110-eV photon energy and 50-cm TOF tube length.

same conditions for the spectrum shown in Figure 3. At this energy, eight classes of ion pair formations are observed. These are: $H^+-H_2^+$, $CH_3^+-SiH_n^+$ ($n = 0-4$), $CH_3^+-SiCH_3^+$, $H^+-CH_n^+$ ($n = 0-3$), $H^+-C_2H_n^+$ ($n = 1-3$), $H^+-SiH_n^+$ ($n = 0-3$), $H^+-SiCH_n^+$ ($n = 0-5$), and $H^+-SiC_2H_n^+$ ($n = 0-3$). The most efficient process at 110 eV is the ion pair formation of $CH_3^+-SiCH_3^+$. In comparison with the PIPICO spectrum of TMS,[5] it is shown that the product ions and the dissociation patterns in the DMS system are quite similar to those in the TMS system studied recently in our laboratory.[5]

Figure 8 shows the PIPICO spectral behaviors at 24, 35, 45, 70, 90, 105, and 115 eV. It is also noticed that each PIPICO

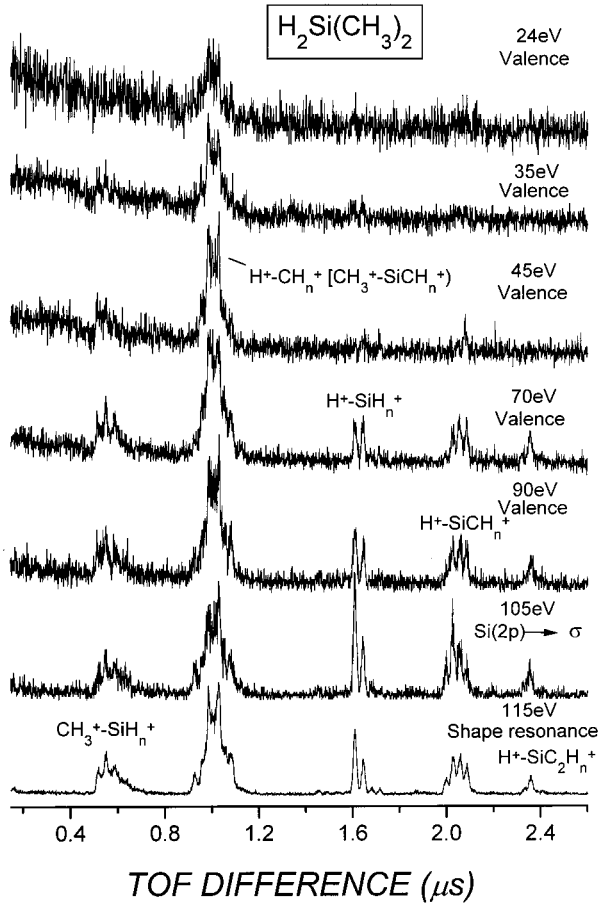

Figure 8. PIPICO spectra of $H_2Si(CH_3)_2$ taken by excitations at photon energies at 24, 35, 45, 70, 90, 105, and 115 eV.

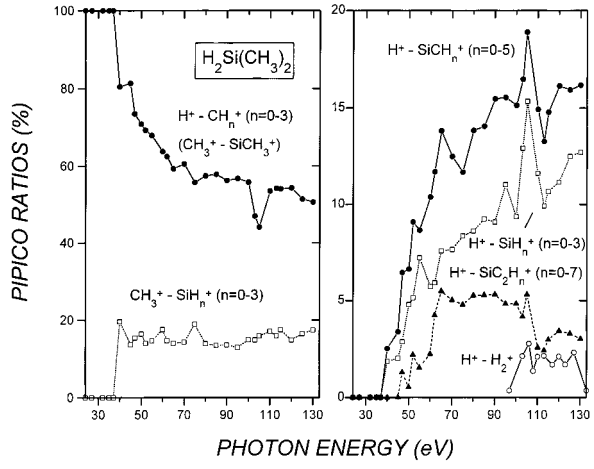

Figure 9. Ratios of integrated intensities of the PIPICO peaks in the TOF mass spectrum of total photoion intensity ($I_{photoion}$:$I_{tot\ photoion}$) in $H_2Si(CH_3)_2$ as a function of photon energy.

spectrum was taken at the same conditions as the PEPICO spectra shown in Figure 4. Figure 9 shows the variation of the PIPICO ratio with energy. Energy dependence of the dissociaton patterns will be discussed later. Figure 10 presents partial PIPICO yield spectra in the range 65−130 eV. It is also noticed that at a given energy, the relative PIPICO yields are derived by multiplying the value for $I_{tot\ PIPICO}$:$I_{tot\ photon}$ by the value for the PIPICO ratio presented in Figure 9. Therefore, the sum of intensities for all the PIPICO spectra indicated in Figure 10 equals the total PIPICO yield displayed in Figure 2. It is also noticed that the two set experiments for the ion yield and

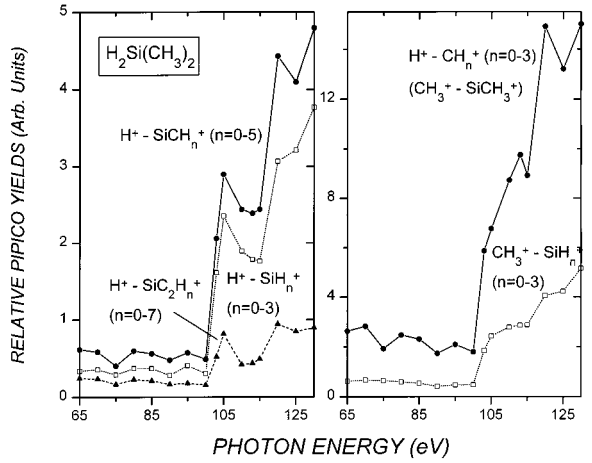

Figure 10. Partial PIPICO yield spectra of $H_2Si(CH_3)_2$ in the range 65−130 eV. The spectral intensities (I_{PIPICO}:$I_{tot\ photoion}$) are presented on the same relative intensity scale.

PIPICO yield measurements (Figures 6 and 10) and for the ion yield ratio and PIPICO ratio measurements (Figures 5 and 9) were performed in consecutive manners for each set experiment under very similar conditions. However, it is found that the measured yield ratios in each set experiment are a little different from each other within experimental uncertainty.

At low energies, the most efficient processes are found to be reactions 1 and 2.

$$H_2Si(CH_3)_2 + h\nu \rightarrow H_2Si(CH_3)_2^+ + e \rightarrow SiCH_5^+ + CH_3 + e \quad (1)$$

$$H_2Si(CH_3)_2 + h\nu \rightarrow H_2Si(CH_3)_2^+ + e \rightarrow SiC_2H_7^+ + H + e \quad (2)$$

Because this molecule includes an equal number of the H atoms and the methyl groups, one can surmise that the efficiencies of the H- and CH_3 eliminations are reflected from the observed ion intensities of $SiC_2H_7^+$ and $SiCH_5^+$, respectively, showing that the efficiencies in the dissociation pathways are similar to each other. Other eliminations of H_2 (or H + H), CH_4 (or CH_3 + H), and H_2 + CH_3 are found to be competitive with processes 1 and 2.

In the Si(2p) excitation and ionization regions, however, resonant multiple and normal Auger processes seem to play an important role in the total ion yield, because PIPICO signals are greatly enhanced in these regions, as seen in Figure 10. The variation of the partial ion yields with energy is discussed below in conjunction with the relevant electronic states, based on the observations of the ion and PIPICO intensities as a function of energy.

H^+ Channel. As seen in Figures 5a and 6a, the H^+ intensity starts to rise from ≈ 102 eV and then reaches a maximum at ≈ 103.4 eV. This spectral feature has also been observed in the TMS system.[5] Around this energy, the PIPICO intensities corresponding to $H^+-SiC_nH_p^+$ ($n = 0-2$) are greatly enhanced. Previous studies of photoabsorption[13] and photoionization[10,11] of SiH_4 show that the transition of Si(2p) to the Si−H antibonding orbital occurs in the range from ≈ 102 eV to ≈ 105 eV. Therefore, it seems a plausible observation that the bond-selective fragmentation involves the ionic bond cleavage of Si−H, such as $H^+-SiC_nH_p^+$ ($n = 0-2$) in the Si(2p)-to-σ^* (Si−H antibonding orbital) transition.

In our simple PIPICO mode, it is impossible to detect three or more ions coincidentally. The formation of the ion pairs $H^+-CH_n^+$ ($n = 0-3$) and $H^+-H_2^+$ hints at the occurrence of triple ionization. Because the electronegativities of H and C atoms are larger that of Si, and because the positive charge prefers the more massive fragment, the silicon-containing cationic species are most likely formed along with the ion pairs of $H^+-CH_n^+$ ($n = 0-3$) and $H^+-H_2^+$ by processes 3 and 4.

$$H_2Si(CH_3)_2^{3+} \rightarrow H^+ + CH_n^+ (n = 0-4) + SiCH_3^+ + NP \quad (3)$$

$$H_2Si(CH_3)_2^{3+} \rightarrow H^+ + H_2^+ + SiC_nH_p^+ (n = 0-2, p = 0-5) + NP \quad (4)$$

Throughout this text, NP denotes the corresponding neutral products as undetected fragments and IP refers to the corresponding ionic products as the unidentified fragments. However, it should be noted that only the observations of the ion pairs of $H^+ + CH_n^+$ ($n = 0-4$), $H^+ + SiCH_3^+$, and CH_n^+($n = 0-4$) + $SiCH_3^+$ cannot confirm the existence of a triply charged parent ion of $H_2Si(CH_3)_2^{3+}$, because each fragmentation pathway would have its own probability to occur from the doubly charged precursor ion.

CH_n^+ ($n = 0-4$) Channel. The ion yield ratio of CH_3^+ begins to increase after ≈ 105 eV and then reaches a maximum at ≈ 110 eV, the energy above the threshold. As seen in Figures 5a and 9, the ion yield ratio for CH_3^+ and the PIPICO ratios for $H^+-CH_n^+$ ($n = 0-4$) ($CH_3^+-SiCH_3^+$), respectively, are found to dip around 105 eV. This indicates that at these energies, the ion pair formations of $H^+-SiC_nH_p^+$ ($n = 0-2$) are quite competitive (Figure 9), demonstrating that the occurrence of the bond-selective fragmentation processes depends on the energy. Previous study of the dissociative ionization of $Si(CH_3)_4$ also shows that the Si−C bond cleavages leading to the ion pair formation of $CH_3^+-Si(CH_3)_n^+$ ($n = 0-3$) occur efficiently at ≈ 107 eV.[12] It is still unknown why the CH_3^+ ion is abundant at the post-threshold energy (≈ 110 eV).

Reactions 5 and 6 can account for the formation of CH_n^+ ($n = 0-4$):

$$H_2Si(CH_3)_2^{2+} \rightarrow CH_3^+ + SiCH_3^+ + H_2 \text{ (or H + H)} \quad (5)$$

$$H_2Si(CH_3)_2^{3+} \rightarrow H^+ + CH_n^+ (n = 0-4) + IP \text{ (or IP + NP)} \quad (6)$$

$C_2H_n^+$($n = 0-4$) Channel. A doubly charged ion cannot be distinguished from the singly charged ion when their mass-to-charge ratios are the same. Therefore, the formation of the ion pair of $H^+-C_2H_n^+$($n = 0-3$) is not clarified, because the mass-to-charge ratios of $C_2H_2^+$, $C_2H_3^+$, and $C_2H_4^+$ are the same as those of SiC_2^{2+}, $SiC_2H_2^{2+}$, and Si^+ ($SiC_2H_4^{2+}$), respectively. However, we strongly believe that processes such as reactions 7 and 8 can occur, because in our laboratory we have observed the $C_2H_n^+$ ($n = 0-4$) ion in the dissociative photoionization of $Ge(CH_3)_4$.[45]

$$H_2Si(CH_3)_2^{2+} \rightarrow H + [H_3Si{\bullet\bullet}|]^{2+} \rightarrow H + SiH_3^+ + C_2H_4^+ \quad (7)$$

$$H_2Si(CH_3)_2^{3+} \rightarrow H^+ + [H_3Si{\bullet\bullet}|]^{2+} \rightarrow H^+ + C_2H_4^+ + SiH_3^+ \quad (8)$$

The formation of SiH_3^+ indicates that intramolecular rearrangement involving the double H-transfers from the carbon atoms to the silicon atom can occur prior to the Si−C bond cleavages. This is discussed further below.

SiH_n^+ ($n = 0-3$) Channel. As seen in Figure 5b, photon energy dependence of the SiH_3^+ ion intensities is quite different from that of Si^+ and SiH^+, implying different sources of the ion formation. It is interesting to infer the reaction mechanism for the formation of SiH_3^+. The formation of the ion indicates the occurrence of the hydrogen migration from carbon to silicon atom.

$$H_2Si(CH_3)_2^+ \rightarrow H + [H_3Si{\bullet\bullet}||]^+ \rightarrow H + SiH_3^+ + C_2H_4 \quad (9)$$

This kind of hydrogen shift and the bond formation between the Si atom and the ethene ligand are reported by previous experimental and theoretical studies.[5,46−49] However, the Si^+ and SiH^+ ions are presumed to be formed directly via the Si−C and Si−H bond cleavages. The ion efficiencies for the Si^+ and SiH^+ ions are greatly enhanced in the Si(2p) excitation and continuum regions. This indicates that the Si(2p) excitation followed by Auger processes weakens specifically the Si−C and Si−H bonds rather than the C−H bonds, giving rise to the observation of the Si^+ and SiH^+ ions. The major channels for the Si^+ and SiH^+ ions are reactions 10−12.

$$H_2Si(CH_3)_2^{2+} \rightarrow CH_3^+ + SiH_n^+ (n = 0-1) + NP \quad (10)$$

$$H_2Si(CH_3)_2^{2+} \rightarrow H^+ + SiH_n^+ (n = 0-1) + NP \quad (11)$$

$$H_2Si(CH_3)_2^{3+} \rightarrow H^+ + CH_3^+ + SiH_n^+ (n = 0-1) + NP \quad (12)$$

$SiCH_n^+$ ($n = 0-5$) Channel. Figure 7 indicates that one of the major dissociation channels leading to the formation of the $SiCH_n^+$ ($n = 0-5$) ions near the Si(2p) threshold may be process 13.

$$H_2Si(CH_3)_2^{2+} \rightarrow H^+ + SiCH_n^+ (n = 0-5) + NP \quad (13)$$

This dissociation behavior near the threshold is contrasted with the behavior of the valence shell region as shown in reaction 1. Specifically, dissociation channel leading to the formation of the $SiCH_3^+$ is found to be process 14 (Figure 7).

$$H_2Si(CH_3)_2^{2+} \rightarrow CH_3^+ + SiCH_3^+ + NP \quad (14)$$

Also, the triple ionization followed by dissociation (process 15) can account for the formation of $SiCH_3^+$

$$H_2Si(CH_3)_2^{3+} \rightarrow H^+ + CH_3^+ + SiCH_3^+ + H \quad (15)$$

because any ion pair from the three product ions is clearly observed in the PIPICO spectra (Figure 7).

$SiC_2H_n^+$ ($n = 0-7$) Channel. As seen in Figure 3, the $SiC_2H_n^+$ ions appear in the two TOF regions. One is for the smaller n (around 1), and the other is for larger n (around 7). We presume that the ions with smaller n are formed via core excitation followed by consecutive eliminations of molecular and/or atomic hydrogen, and that those with the larger n are produced in the off-resonance valence ionization region. Comparing the ions detected in the PIPICO mode with those in the PEPICO mode, we found that the ions $SiC_2H_n^+$ ($n > 3$) are absent in the PIPICO spectra (Figures 7 and 8), in contrast with their existence in the PEPICO spectra, as seen in Figures 3 and 4. This implies that a new dissociation pattern, other than dissociation of doubly and multiply charged ions, must be responsible for the formation of $SiC_2H_n^+$ ($n > 3$):

SCHEME 1

$$\begin{aligned}
H_2Si(CH_3)_2 + h\nu &\rightarrow H_2Si^*(CH_3)_2 \ \text{(core excitation)}\\
H_2Si^*(CH_3)_2 &\rightarrow H_2Si(CH_3)_2^{2+} + 2e\\
&\rightarrow H_2Si(CH_3)_2^{3+} + 3e\\
H_2Si(CH_3)_2^{2+} &\rightarrow CH_3^+ + SiCH_3^+ + H_2\\
&\rightarrow \cdots\\
H_2Si(CH_3)_2^{3+} &\rightarrow H^+ + CH_3^+ + SiCH_3^+ + H\\
&\rightarrow \cdots
\end{aligned}$$

$$H_2Si^*(CH_3)_2 \rightarrow H + HSi^*(CH_3)_2 \rightarrow H + HSiC_2H_n^+ (n > 3) + NP + e \quad (16)$$

In previous studies of core excitation of silane, de Souza et al.[10] proposed a two-step decay process for a valence resonance, namely a fast dissociation followed by the autoionization of the excited fragment, on the basis of the observation of Br(3d) core excitation of HBr.[50]

Interestingly, one can observe consecutive molecular eliminations leading to the observations of the various ions of $SiC_2H_n^+$ (n = odd number 1, 3, 5, 7), as seen in Figure 5c. In the whole energies, the $SiC_2H_n^+$ (n = odd number) ions are formed more efficiently than those having the corresponding even numbers. If the several consecutive eliminations of molecular hydrogen are responsible for the observed ions, the weak intensities of $SiC_2H_n^+$ (n = even number) are probably related to the intensity of $SiC_2H_6^+$ being lower than that of $SiC_2H_7^+$, given that the ions $SiC_2H_n^+$($n = 6, 7$) are presumed to be a start species for the consecutive H_2 elimination processes.

According to the PIPICO spectrum (Figure 7), one can suggest that the dissociation pathways of the core-excited DMS lead to the formations of the observed ions. Scheme 1 outlines the plausible dissociative ionization processes of DMS, on the basis of the PIPICO measurements.

Conclusions

Fragmentation processes following valence and Si(2p) core electron excitation/ionization of $H_2Si(CH_3)_2$ have been investigated in the range of 24−133 eV by means of the PEPICO and PIPICO techniques coupled to synchrotron radiation. In the valence ionization region, specially $E < 30$ eV, eliminations of H, H_2, CH_3, CH_4 (or H + CH_3), and CH_3 + H_2 (or H + CH_4) are observed predominantly leading to the formation of $SiCH_n^+$ ($n = 3-5$) and $SiC_2H_n^+$ ($n = 6, 7$). Both the total photoionization and PIPICO yield curves of $H_2Si(CH_3)_2$ have revealed significant features below the Si(2p) threshold (≈ 103.4 eV). The HF/6-311++G(2df,p) orbital energy calculation indicates that the energy corresponds to the $Si(2p_{1/2})$ -to-$\sigma(1A_1)$* transition. Around this energy, the H^+ intensity reaches a maximum, and the PIPICO intensities corresponding to $H^+ - SiC_nH_p^+$ ($n = 0-2$, $p = 0-7$) are greatly enhanced, revealing that the bond-selective dissociation processes involving the H−Si bonds occur. Above the threshold, we observe a small feature in the total ion yield curve, which may correspond to a shape resonance near 107.6 eV, and also a slow rise above 109 eV assigned to a delayed onset phenomena and/or to photoionization shake-off. In this region, the coincident ion pair formation of H^+−

CH_n^+ ($n = 0-3$) prevails, indicating that the possibility of triple ionization followed by molecular fragmentation is greatly enhanced.

Acknowledgment. The authors wish to acknowledge the financial support of the Korea Research Foundation, made in the international collaborative research program of 1997. The members of the UVSOR facility at the Institute for Molecular Science in Okazaki, Japan, are greatly acknowledged for their valuable help. Computations were carried out by using the CRAY C90 of the SERI Supercomputer Center in Korea, which is gratefully acknowledged.

References and Notes

(1) Bodeur, S.; Millié, P.; Lugrin, E. L.; Nenner, I.; Filipponi, A.; Boscherini, F.; Mobilio, S. *Phys. Rev. A* **1989**, *39*, 5075.
(2) Bodeur, S.; Millié, P.; Nenner, I. *Phys. Rev. A* **1990**, *41*, 252.
(3) Sutherland, D. G. J.; Kasrai, M.; Bancroft, G. M.; Liu, Z. F.; Tan, K. H. *Phys. Rev. B* **1993**, *48*, 14989.
(4) Boo, B. H.; Park, S. M.; Koyano, I. *J. Phys. Chem.* **1995**, *99*, 13362.
(5) Boo, B. H.; Lee, S. Y.; Kim, H.; Koyano, I. *J. Phys. Chem.* **1996**, *100*, 523.
(6) Boo, B. H.; Park, S. M.; Koyano, I. *J. Korean Phys. Soc.* **1998**, *32*, 513.
(7) Boo, B. H.; Liu, Z.; Lee, S. Y.; Koyano, I. *J. Phys. Chem.* **1998**, *102*, 8261.
(8) Lablanquie, P.; Souza, A. C. A.; de Souza, G. G. B.; Morin, P.; Nenner, I. *J. Chem. Phys.* **1989**, *90*, 7078.
(9) de Souza, G. G. B.; Morin, P.; Nenner, I. *J. Chem. Phys.* **1989**, *90*, 7071.
(10) de Souza, G. G. B.; Morin, P.; Nenner, I. *Phys. Rev. A* **1986**, *34*, 4770.
(11) Yagishita, A.; Arai, S.; Brion, C. E.; Hayaishi, T.; Murakami, J.; Sato, Y.; Ukai, M. *Chem. Phys. Lett.* **1986**, *132*, 437.
(12) Morin, P.; de Souza, G. G. B.; Nenner, I.; Lablanquie, P. *Phys. Rev. Lett.* **1986**, *56*, 131.
(13) Hayes, W.; Brown, F. C. *Phys. Rev. A* **1972**, *6*, 21.
(14) Bozek, J. D.; Tan, K. H.; Bancroft, G. M.; Fu, K. J. *Chem. Phys.* **1991**, *158*, 171.
(15) Winkler, D. C.; Moore, J. H.; Tossell, J. A. *Chem. Phys. Lett.* **1994**, *222*, 1.
(16) Nagaoka, S.; Ohshita, J.; Ishikawa, M.; Takano, K.; Nagashima, U.; Takeuchi, T.; Koyano, I. *J. Chem. Phys.* **1995**, *102*, 6078.
(17) Imamura, T.; Brion, C. E.; Koyano, I.; Ibuki, T.; Masuoka, T. *J. Chem. Phys.* **1991**, *94*, 4936.
(18) Sutherland, D. G. J.; Bancroft, G. M.; Tan, K. H. *J. Chem. Phys.* **1992**, *97*, 7918.
(19) Bozek, J. D.; Bancroft, G. M.; Tan, K. H. *Phys. Rev. A* **1991**, *43*, 3597.
(20) Friedrich, H.; Pittel, B.; Rabe, P.; Schwarz, W. H. E.; Sonntag, B. *J. Phys. B: At. Mol. Opt. Phys.* **1980**, *13*, 25.
(21) Simon, M.; Lebrun, T.; Martins, R.; de Souza, G. G. B.; Nenner, I.; Lavollee, M.; Morin, P. *J. Phys. Chem.* **1993**, *97*, 5228.
(22) Ishikawa, H.; Fujima, K.; Adachi, H.; Miyauchi, E.; Fujii, T. *J. Chem. Phys.* **1991**, *94*, 6740 and references therein.
(23) Tse, J. S.; Liu, Z. F.; Bozek, J. D.; Bancroft, G. M. *Phys. Rev. A* **1989**, *39*, 1791.
(24) Sodhi, R. N. S.; Daviel, S.; Brion, C. E.; de Souza, G. G. B. *J. Electron Spectrosc. Relat. Phenom.* **1985**, *35*, 45.
(25) Vinogradov, A. S.; Zimkina, T. M. *Opt. Spektrosk. (USSR)* **1971**, *31*, 288.
(26) Zimkina, T. M.; Vinogradov, A. S. *J. Phys. (Paris) Colloq.* **1971**, *32*, C4−3.
(27) Nagaoka, S.; Ohshita, J.; Ishikawa, M.; Masuoka, T.; Koyano, I. *J. Phys. Chem.* **1993**, *97*, 1488.
(28) Chen, J. M.; Lu, K. T.; Liu, R. G.; Lay, J. W.; Liu, Y. C. *J. Chem. Phys.* **1997**, *106*, 9105.
(29) Larkin, F. P.; McColl, J.; Chelkowska, E. Z. *J. Electron Spectrosc. Relat. Phenom.* **1994**, *67*, 275.
(30) Cooper, G.; Ibuki, T.; Brion, C. E. *Chem. Phys.* **1990**, *140*, 147.
(31) Schwarz, W. H. E. *Chem. Phys.* **1975**, *11*, 217.
(32) Nagaoka, S.; Mase, K.; Nagasono, M.; Tanaka, S.; Urisu, T.; Ohshita, J. *J. Chem. Phys.* **1997**, *107*, 10751.
(33) Masuoka, T.; Horigome, T.; Koyano, I. *Rev. Sci. Instrum.* **1989**, *60*, 2179.
(34) Ishiguro, E.; Suzui, M.; Yamazaki, J.; Nakamura, E.; Sakai, K.; Matsudo, O.; Mizutani, N.; Fukui, K.; Watanabe, M. *Rev. Sci. Instrum.* **1989**, *60*, 2105.
(35) Masuoka, T.; Koyano, I. *J. Chem. Phys.* **1991**, *95*, 909.
(36) Masuoka, T.; Koyano, I.; Saito, N. *Phys. Rev. A* **1991**, *44*, 4309.
(37) Pierce, L.; Petersen, D. H. *J. Chem. Phys.* **1960**, *33*, 907.
(38) Schwarz, W. H. E.; Buenker, R. J. *Chem. Phys.* **1976**, *13*, 153.
(39) Frisch, M. J.; Trucks, G. W.; Schlegel, H. B.; Gill, P. M. W.; Johnson, B. G.; Robb, M. A.; Cheeseman, J. R.; Keith, T.; Petersson, G. A.; Montgomery, J. A.; Raghavachari, K.; Al-Laham, M. A.; Zakrzewski, V. G.; Ortiz, J. V.; Foresman, J. B.; Cioslowski, J.; Stefanov, B. B.; Nanayakkara, A.; Challacombe, M.; Peng, C. Y.; Ayala, P. Y.; Chen, W.; Wong, M. W.; Andres, J. L.; Replogle, E. S.; Gomperts, R.; Martin, R. L.; Fox, D. J.; Binkley, J. S.; Defrees, D. J.; Baker, J.; Stewart, J. P.; Head-Gordon, M.; Gonzalez, C.; Pople, J. A. *Gaussian 94*, Revision D.2; Gaussian, Inc: Pittsburgh, PA, 1995.
(40) Streubel, P.; Franke, R.; Chasse, T.; Fellenberg, R.; Szargan, R. *J. Electron Spectrosc. Relat. Phenom.* **1991**, *57*, 1.
(41) Fano, U.; Cooper, J. W. *Rev. Mod. Phys.* **1968**, *40*, 441.
(42) Manson, S. T. *Adv. Electron. Phys.* **1976**, *41*, 73.
(43) Carlson, T. A.; Nestor, C. W., Jr. *Phys. Rev. A* **1973**, *8*, 2887.
(44) Mukoyama, T.; Taniguchi, K. *Phys. Rev. A* **1987**, *36*, 693.
(45) Boo, B. H.; Saito, N.; Suzuki, I. H.; Koyano, I., to be submitted for publication.
(46) Groenewold, G. S.; Gross, M. L.; Bursey, M. M.; Jones, P. R. *J. Organomet. Chem.* **1982**, *235*, 165.
(47) Bakhtiar, R.; Holznagel, C. M.; Jacobson, D. B. *Organometallics* **1993**, *12*, 621.
(48) Bakhtiar, R.; Holznagel, C. M.; Jacobson, D. B. *Organometallics* **1993**, *12*, 880.
(49) Willard, B. B.; Graul, S. T. *J. Phys. Chem.* **1998**, *102*, 6942.
(50) Morin, P.; Nenner, I. *Phys. Rev. Lett.* **1986**, *56*, 1913.